Separation and Purification Technology 373 (2025) 133520

Contents lists available at ScienceDirect

Separation and Purification Technology

journal homepage: www.elsevier.com/locate/seppur

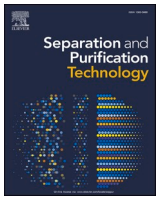

Optimized microfluidic platform for the selective recovery of critical materials from aqueous mixtures

Christian Fernández-Maza, Gloria González-Lavín, Lucía Gómez-Coma, Marcos Fallanza, Inmaculada Ortiz *

Departamento de Ingenierías Química y Biomolecular, Universidad de Cantabria, Av. Los Castros s/n, 39005 Santander, Spain

A R T I C L E I N F O

Editor: Luo Guangsheng

Keywords:
Microfluidic platform
Multiphase reaction
Process design
Rare earths microextraction

A B S T R A C T

This work reports the optimization strategy for the design of a microfluidic platform to achieve the separation and recovery of aqueous mixtures of rare earth elements (REEs); the work showcases the separation of dysprosium, neodymium and lanthanum using microextraction modules with an organic phase constituted of Cyanex® 572 diluted in Shellsol® D70. An optimization model has been developed to assist in the design of the number of stages (microextractors, settling tanks and mixer and splitter units) and the best operational conditions that maximize the separation and recovery targets. Results predicted by the model with a configuration composed of 4 microreactors have been experimentally evaluated.

Starting with 1 mM equimolar REE mixtures and 301 mM Cyanex® 572 as the organic phase, the model shows that REE recovery and concentration improve with an increasing number of microextractors. Using eight microextractors, along with optimised pH and recycling, recoveries exceed 92 %, purities reach 93 %, and concentrations are at least six times higher than the feed.

The REEs extraction microfluidic platform has been 3D printed with a modular LEGO® type design that facilitates reconfiguration and scalability. Together with the optimisation model, this platform represents a valuable tool for the design and implementation of future critical element mixtures microextraction applications.

1. Introduction

Microfluidics offers a promising platform for reactive extraction processes due to its superior control over mass transport phenomena, efficient phase contact and improved selectivity compared to conventional extraction methods [1]. This technology enables precise manipulation of fluids at the microscale, resulting in significantly higher mass transfer rates, shorter diffusion distances, minimised reagent consumption and reduced waste generation [2,3]. These advantages make microfluidics an increasingly attractive alternative for separation processes, including the recovery of metals and rare earth elements (REEs). For instance, Farahani et al. [4] studied the performance of the solvent extraction of Cd ions using a Y-Y microfluidic device, achieving higher mass transfer rates than with batch extractors, with 99.3 % of extraction percentage obtained for a residence time of 8 s, 75 times faster compared to the batch system. This is because microfluidics offers a high surface-to-volume ratio and short diffusion distances.

Other authors, such as Zhou et al. [5], have developed a microfluidic process for the extractive recovery of NCM (Lithium Nickel Manganese Cobalt Oxides) battery materials using a mixed extractant in the organic phase to improve the extraction performance, achieving high recoveries of Mn, Co, Ni and Li of 99.9 %, 98.6 %, 99.5 % and 90 %, respectively. Also, Abdollahi et al. [6] proposed a systematic method for the efficient separation of species with a low separation factor using a Y-Y microdevice, achieving 62 % extraction of Ca^{2+} from an aqueous solution of picric acid and $CaCl_2$. Wouters et al. [7] analysed experimentally the extraction of cobalt from an aqueous phase composed of Ni and Co (3:0.3 $mol{\cdot}l^{-1}$ Ni:Co), using an organic phase with Cyanex® 272 as extractant in a 3D spiral microdevice, achieving 60 % of extraction and a very high separation factor (>1000).

Different authors have reported higher yields in microextraction processes using a multiphasic microdevice given the substantial increase in the interfacial area between the continuous and dispersed phases in microfluidic reactors. Wen et al. [8] studied the mass transfer at the molecular level with different flow regimes, recovering chromium and vanadium by reactive extraction in a microdevice with dispersed droplet and slug generation, thereby increasing the efficiency of mass transfer.

* Corresponding author.
E-mail address: ortizi@unican.es (I. Ortiz).

https://doi.org/10.1016/j.seppur.2025.133520
Received 18 March 2025; Received in revised form 2 May 2025; Accepted 11 May 2025
Available online 12 May 2025

Nomenclature

Roman symbols

C	molar concentration (kmol·m^{-3})
E	percentage of REE extraction (–)
F	molar flow rate (mol·day^{-1})
H	holdup ratio (%)
K_c	equilibrium constant (–)
Q	fluid flow rate (ml·min^{-1})
R	flow rate ratio (–)
Z	objective function (–)

Subscripts

0	initial condition (–)
AP	aqueous phase (–)
in	inlet (–)
OP	organic phase (–)
out	outlet (–)
q	fluid phase (–)

Superscripts

H^+	hydrogen proton (–)
$(HA)_2$	dimer of Cyanex® 572 (–)
i	species (–)
M^{3+}	trivalent metal ion of REE (–)
$MA_3(HA)_3$	complex formed between REE ion and 3 dimers of Cy-572 (–)

Similarly, Cui K. and Huang K. [9] evaluated the separation process of Er (III) and Al(III) using a Y-junction microfluidic device, increasing the interfacial area with enlarged droplets (slugs) of the aqueous phase. Chen et al. [10] reported the extraction of Nd using a hollow droplet generation microdevice (gas-liquid-liquid system) and analysed the influence of residence time and phase ratio; in the analysed conditions the extraction equilibrium of Nd is achieved in 1.3 s in a microfluidic device with a channel length of 0.3 m.

Elements such as dysprosium (Dy), neodymium (Nd) and lanthanum (La) are key to the manufacture of high-tech devices such as permanent magnets [11], rechargeable batteries [12], catalysts [13], displays [14], wind turbines [15] and electric vehicles [16]. These REEs present unique magnetic, catalytic and optical properties that make them irreplaceable for several critical applications [17], making their separation and recovery from secondary sources (waste materials) essential [18]. Microfluidic platforms have emerged as an efficient alternative to investigate these separations due to their ability to integrate multiple functions in miniaturised devices; some authors have used this type of platforms with applications in different fields such as biotechnology, medicine or chemical extraction [19–22]. This feature not only reduces the separation time but also minimises reagent and resource consumption.

After rigorous CFD-assisted design of individual microfluidic device to achieve high extraction performance, this work presents the development and optimisation of a modular microfluidic platform for the separation of an aqueous mixture of REEs (Dy, Nd and La) as a case study. The separation process of a ternary mixture of REEs was selected as a case study, carried out through multiple microextraction and back-extraction steps using a multi-building block platform. It is remarkable that the complexity of the decision-making process increases with the number of stages. Therefore, it is essential to develop a mathematical model that optimises the entire process, considering all the decision variables involved, and to provide a theoretical framework to assist in the design and fabrication of the modular platform adaptable to different separation configurations.

2. Mathematical model

Mathematical model, developed with the Aspen Custom Modeler® V.14 simulation software, is constituted of mass conservation and species transport equations for each block; the optimal solution is achieved using the optimisation tool of the Aspen® software, following the FeasOpt optimiser with a solution convergence tolerance of 0.002.

2.1. Extraction and Back-Extraction blocks

These blocks correspond to spiral shaped microfluidic devices that generate microdroplets in which the extraction and back-extraction reactions of REEs take place, depending on the pH value of the aqueous phase. It is assumed that the residence time inside the microdevices is high enough to reach chemical equilibrium.

The conservation of mass in these blocks is described by the continuity equation for each phase "q":

$$Q_q^{in} = Q_q^{out} \tag{1}$$

where "Q^{in} and Q^{out}" represent the flow rates at the inlet and outlet, respectively for each phase "q".

The species transport equations for rare earth elements "M^{3+}" and protons "H^+" in the aqueous phase and for Cyanex® 572 "$(HA)_2$" and the complex species "$MA_3(HA)_3$" in the organic phase can be written as follows:

$$F_q^i = Q_q^i \cdot C_q^i \tag{2}$$

$$F^{M^{3+}} = F_0^{M^{3+}} - \left(F^{MA_3(HA)_3} - F_0^{MA_3(HA)_3}\right) \tag{3}$$

$$F^{H^+} = F_0^{H^+} + 3\left(F^{MA_3(HA)_3} - F_0^{MA_3(HA)_3}\right) \tag{4}$$

$$F^{(HA)_2} = F_0^{(HA)_2} - 3\left(F^{MA_3(HA)_3} - F_0^{MA_3(HA)_3}\right) \tag{5}$$

$$F^{MA_3(HA)_3} = K_c^{M^{3+}} F^{M^{3+}} \left(\frac{F^{(HA)_2}}{F^{H^+}}\right)^3 \tag{6}$$

where "F_0" and "F" are the initial and equilibrium molar flow rate of each species, calculated with eq. (2), and "$K_c^{M^{3+}}$" represents the equilibrium constant of each rare earth element as given by eq. (14).

2.2. Mixing blocks

In these blocks the mixing of the different streams, both aqueous and organic phases, takes place. It is assumed that the mixing of inlet streams is complete at the outlet of the block.

The conservation of mass is described by the continuity equation for each phase "q", the flow rate at the outlet is equal to the sum of the inlet flow rates, described as:

$$\sum_{in} Q_q^{in} = Q_q^{out} \tag{7}$$

The species conservation equation for each phase "q" can be represented by:

$$\sum_{in} Q_q^{in} \cdot C_q^{i,in} = Q_q^{out} \cdot C_q^{i,out} \tag{8}$$

where "Q^{in} and Q^{out}" represent inlet and outlet flow rates, respectively, "C" is the concentration of species "i" in the phase "q".

2.3. Splitter blocks

In these blocks, splitting of both the aqueous phase and the organic

phase takes place. At the outlet of the block, the inlet stream is divided into two or more streams with different flow rates according to the established flow rate ratio.

The mass conservation equation is described by the continuity equation for each phase "q" as follows:

$$Q_q^{in} = \sum_{out} Q_q^{out} \cdot R_q^{out} \tag{9}$$

$$\sum_{out} R_q^{out} = 1 \tag{10}$$

where "R" is the flow rate ratio of phase "q" for each splitter outlet "*out*".

The species conservation equation for each phase "q" in the splitter blocks can be described as:

$$C_q^{i,out} = C_q^{i,in} \tag{11}$$

The proposed set of equations is able to describe the separation of a ternary mixture of Dy, Nd and La with a concentration 1 mM each from an aqueous solution at pH 1 and flowing at a flow rate of 1 ml·min^{-1}. The procedure is subjected to the following limitations:

The flow rates of the streams must be higher than zero ($Q \geq 0$); therefore, recirculation ratios in the separation stages are between 0 and 1 ($0 \leq R \leq 1$).

The concentration of each element is positive ($C \geq 0$).

The aqueous phase holdup (H_{AP}) in the extraction and back-extraction stages is between 30 % and 70 % to ensure efficient generation of microdroplets in the microdevice (30 % $\leq H_{AP} \leq$ 70 %) [1].

The objective function of the optimisation model maximises the productivity and purity of each element in its respective outlet stream according to equation (12):

$$Z_{max} = \sum_i \left(Q_{AP}^{i,out} \cdot C_{AP}^{i,out} \cdot \frac{C_{AP}^{i,out}}{\sum_i C_{AP}^{i,out}} \right) \tag{12}$$

3. Materials and methods

3.1. Equilibrium study

The equilibrium constant (K_c) of the reaction between rare earth elements (M^{3+}) and the Cyanex® 572 extractant ($(HA)_2$) was determined experimentally in conventional mixer-settlers; 10 ml of an aqueous phase ($[Dy^{3+}] = [Nd^{3+}] = [La^{3+}] = 1$ mM and pH $\leq$ 2.5) were contacted with 10 ml of the organic phase ($[(HA)_2] = 301$ mM in Shellsol® D70) under stirring at room temperature (24 ± 2 °C). After equilibrium had been reached the liquid phases were separated by decantation and samples (1 ml of aqueous phase) were taken. Then the REEs concentration was measured in the Agilent® 4210 Microwave Plasma Atomic Emission Spectrometer at a wavelength of 353.2, 430.4 and 394.9 nm for dysprosium, neodymium and lanthanum, respectively, calculating the percentage of REE extraction ("E") from the concentration values in the aqueous phase as:

$$E = \frac{C_0^{M^{3+}} - C^{M^{3+}}}{C_0^{M^{3+}}} \tag{13}$$

where "$C_0^{M^{3+}}$" is the original REE concentration (kmol·m^{-3}) in the aqueous phase before the extraction and "$C^{M^{3+}}$" the REE concentration in the aqueous medium (kmol·m^{-3}) after extraction.

3.2. Design of LEGO® type microfluidic platform

The design of the microdevices is based on a detailed study using Computational Fluid Dynamics (CFD), developed in previous works [1,2], which allowed the evaluation of the influence of both the geometric characteristics of the devices and the operating variables on their performance. The methodology employed in this stage is schematically illustrated in Fig. 1, where the design is iteratively adjusted and refined through CFD simulations in order to improve the performance under specific operating conditions.

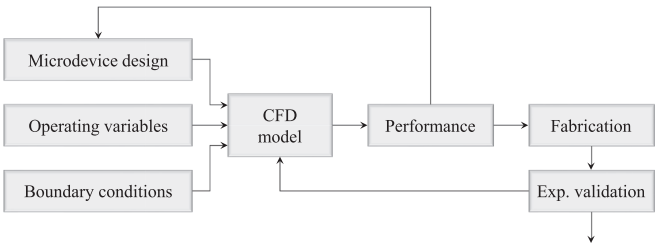

Fig. 1. Flow diagram of the CFD-assisted design stage of microfluidic devices.

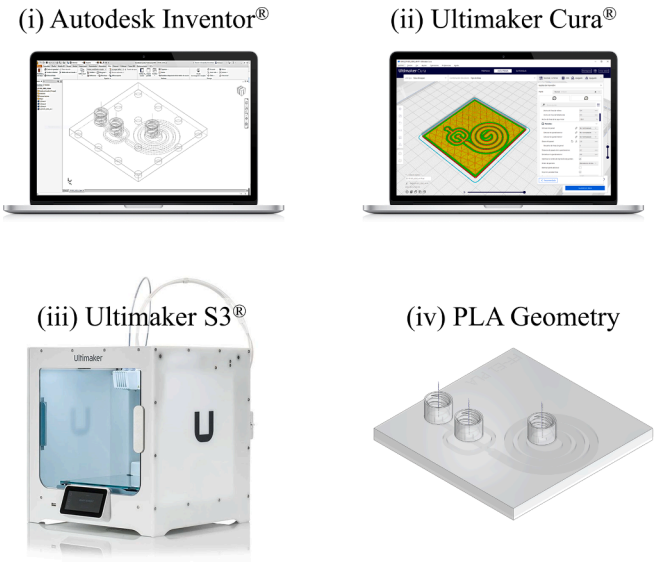

Fig. 2. Schematic representation of the design and fabrication sequence of microfluidic devices by means of one-step additive manufacturing techniques.

Once the design satisfies performance requirements according to CFD predictions, it is fabricated using 3D printing techniques and subsequently validated through experimental trials.

This approach has been used to evaluate a methodology for designing a modular microfluidic platform based on a flexible assembly that can be tailored to specific separation goals.

To create this modular microfluidic platform, a structured support has been designed in Autodesk Inventor® with LEGO® style studs, allowing expansion through puzzle-like interlocking joints. The microfluidic devices are designed with a perforated base that fits over the base studs, providing a highly modular platform. This feature allows the devices to be placed in any position on the base, facilitating modification and expansion of the configuration according to the needs of the process.

Several specific types of microfluidic devices have been developed for the separation of REEs: Spiral microreactors (i) are designed to carry out the extraction and back-extraction stages of REEs, with a microchannel geometry identical to that analysed in a previous work [1]. At the outlet of these microreactors, settling tanks (ii) are used to separate the aqueous and organic phases. To ensure proper conditioning of the streams, mixers (iii) are incorporated to combine streams of the same phase and to adjust the pH as required. Finally, splitters (iv) are incorporated to divide a single stream into multiple streams, allowing recirculation and improving process control.

The base was fabricated using additive manufacturing techniques with 3D printing directly on the Ultimaker® S3 with AA 0.4 Print Core (Ultimaker®). Similarly, the microfluidic devices were 3D printed in a

single step using transparent PLA (Ultimaker®) filament material to visualise the inner part of the devices, as shown in Fig. 2.

3.3. Design of a multistage microfluidic extraction process for the separation of multicomponent REE mixtures

For the design of the microfluidic platform, the mathematical model described is implemented in the Aspen Custom Modeler® software. In this model, the different blocks that constitute the platform are simulated, including the microfluidic devices where the extraction and back-extraction stages of REEs are carried out, as well as mixers and splitters for streams recycling and pH adjustment in the process. Fig. 3 presents the superstructure illustrating the configuration of a three-element microfluidic separation process, using 8 microreactors, half for extraction of REEs and half for back-extraction of REE, with all possible process streams from both organic (red lines) and aqueous (blue lines) phases. The aqueous stream (Fig. 3.a, mixture of Dy, Nd and La) enters the first extraction microreactor (E1) where the main part of dysprosium is separated. This stream with the extracted Dy undergoes a back-extraction process in unit R1 using an acidic stream (Fig. 3.c), resulting in a Dy-rich stream leaving the system (Fig. 3.i). The aqueous stream leaving E1, enriched in neodymium and lanthanum, is subjected to pH adjustment by addition of a basic stream (Fig. 3.b) to maximise Nd extraction and minimise La extraction in the next two microextractors, E2 and E3.

The Nd-rich organic stream is then back-extracted in units R2 and R3, leaving a Nd-rich aqueous stream (Fig. 3.j) at the end of the process. Finally, the residual aqueous stream enriched in La, at the outlet of E3, is subjected to a further pH adjustment to extract lanthanum in the microextractor E4, followed by its back-extraction in R4. This allows lanthanum to be concentrated in an aqueous stream (Fig. 3.k), while the final AP leaves the system practically free of rare earth elements (Fig. 3.h).

It is worth mentioning the need for multiple recycling streams within the process, which needs the implementation of mixing blocks and splitters. Although these additions increase the complexity of the system, they contribute significantly to improve its overall performance. The model is designed to determine the overall microfluidic platform topology and the operating conditions of each stage that maximise the separation of REEs from multicomponent mixtures.

4. Results and discussion

4.1. Extraction equilibria in multicomponent solutions

The analysis of the extraction of Dy(III), Nd(III), and La(III) from an acidic aqueous phase into an organic phase using the extractant Cyanex® 572 was conducted through a reactive multiphase cation exchange process. The use of this extractant proves advantageous due to its high selectivity and extraction capacity, making it a valuable choice for separating and purifying rare earth elements from complex mixtures [23]. This method takes advantage of Cyanex® 572′s selective affinity for trivalent REEs in acidic environments, facilitating their transfer from the aqueous to the organic phase. The extraction follows a specific stoichiometry, where the metal ions react with the active components of the extractant to form metal-extractant complexes. These complexes are then solubilized in the organic phase, effectively separating the REEs from the aqueous solution. The underlying mechanism is based on acid-base equilibrium reactions where the trivalent rare earth ions replace protons from the extractant molecules, allowing selective transfer to the organic phase depending on their ionic radius and acidity [24].

In this context, M^{3+} represents the trivalent REEs such as Dy^{3+}, Nd^{3+}, and La^{3+}. The notation $(HA)_2$ refers to the dimeric form of the Cyanex® 572 extractant, which is dissolved in the organic solvent Shellsol® D70. The species $MA_3(HA)_3$ is the organic complex species formed between the single REE ion and three dimers of Cy-572 (Cyanex® 572) in the organic phase.

The formation of the $MA_3(HA)_3$ complex species occurs through a cation exchange reaction, where the trivalent RE ion (M^{3+}) binds to the Cyanex® 572 dimers, releasing protons (H^+) into the aqueous phase. The bars over the species indicate that these complexes reside in the organic phase. The extraction process can be expressed by the following reaction [25]:

$$M^{3+} + 3\overline{(HA)_2} \leftrightarrow \overline{MA_3(HA)_3} + 3H^+ \quad \text{(R1)}$$

This stoichiometric relationship highlights the role of Cyanex® 572 in facilitating the cation exchange mechanism, where the REEs are exchanged with protons from the extractant, forming stable metal-extractant complexes.

According to previous references [25], the equilibrium constant (K_c) of (R1) can be simplified and expressed by the mass action law eq. (14),

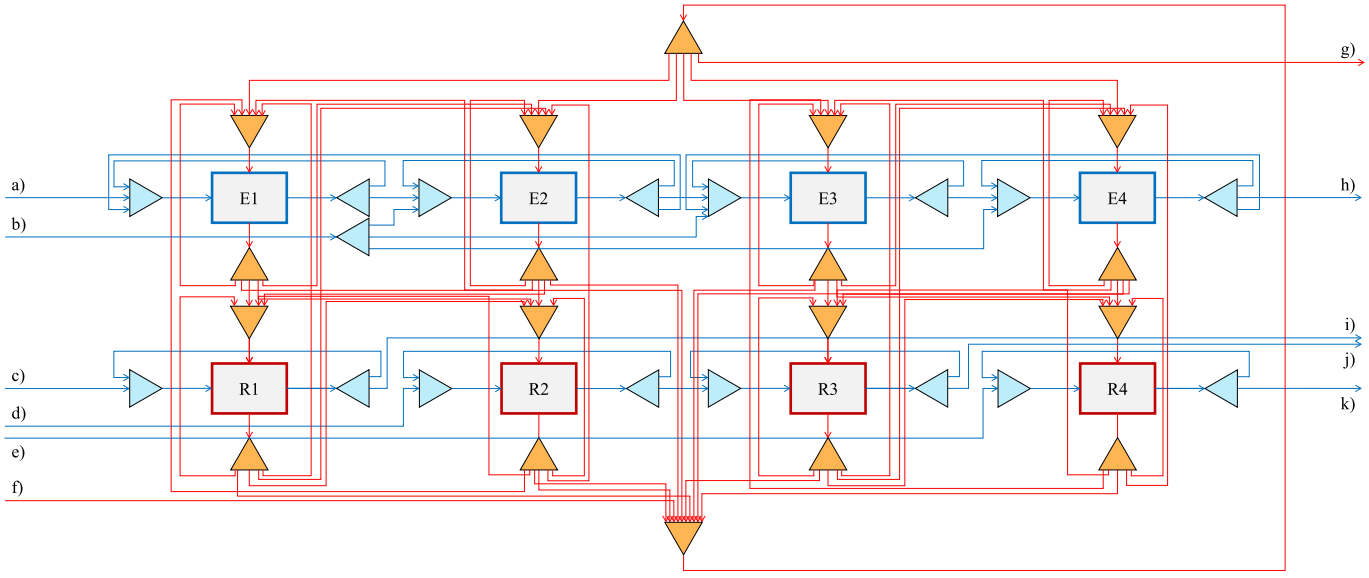

Fig. 3. Superstructure of the microfluidic platform of REEs extraction-back-extraction process. (a) is the inlet of the feed aqueous solution, (b) represents the inlet of the pH adjustment stream, (c), (d), and (e) are the inlets of aqueous acidic streams for the back-extraction of REEs, (f) and (g) represent the inlet and outlet of the OP, respectively, (h) is the outlet of AP without REEs, (i), (j) and (k) are the outlet streams concentrated in Dy^{3+}, Nd^{3+} and La^{3+}, respectively.

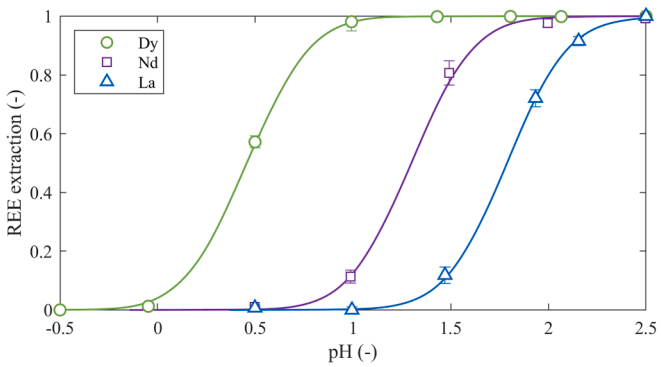

Fig. 4. Equilibrium isotherms of REEs at different pH values, obtained with 301 mM of $(HA)_2$ in Shellsol® D70 and 1 mM of M^{3+} as chlorides, where dots and lines represent the experimental and simulated data, respectively.

where "K_c" is calculated as follows:

$$K_c = \frac{\overline{[MA_3(HA)_3]}\cdot[H^+]^3}{[M^{3+}]\cdot\overline{[(HA)_2]}^3} \quad (14)$$

According to the previously described procedure, the corresponding calculations were carried out to obtain the equilibrium constant (K_c) of the extraction of REEs, obtaining the following dimensionless values: 1.5 for dysprosium, $4.8{\cdot}10^{-3}$ for neodymium and $1.6{\cdot}10^{-4}$ for lanthanum. With these results, it is possible to estimate the extraction isotherms at different pH values, which have been experimentally verified by means of batch experiments using an initial concentration of 1 mM of each REE and an initial concentration of extractant (Cyanex® 572) of 301 mM.

Fig. 4 depicts the extraction isotherms of these three elements showing the influence of the pH of the aqueous phase on the extraction equilibrium. pH is a crucial variable to design and achieve the selective separation of the elements. At a specific pH, each element shows different affinity for the extractant, which facilitates their individualisation and recovery from the mixture.

The study demonstrates that by modifying the pH of the aqueous solution, it is possible to optimise the conditions to extract each element selectively, maximising the purity and separation of the multicomponent mixtures.

4.2. CFD-assisted design of microfluidic device

In the design stage of the microdevices, an exhaustive study was carried out using CFD, focusing on the evaluation of the influence of the geometrical characteristics of the devices and the operating variables on their performance. This methodology, developed and applied in previous works [1,2], allowed the microfluidic system to be known and configured in order to improve its performance under specific operating conditions. The generation of droplets by flow focusing configuration, combined with the curved geometry of the spiral shape microchannel, increases the interfacial area and promotes the mixing of reagents thanks to the formation of Dean vortices. This ensures a continuous supply of reagents to the interface, leading to improved performance of the extraction process. The design of the microdevice determines the influence of several key parameters on the extraction performance of each of the elements of interest. These parameters include the total length of the microchannel, their radii of curvature, the size of the droplets generated, the holdup value, the input flow rates of each phase, the composition of the organic phase (in this case with a Cyanex® 572 concentration of 301 mM in Shellsol® D70), and the acidity of the aqueous phase [1].

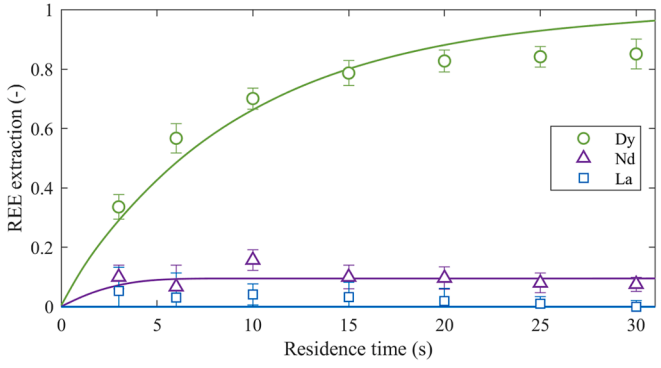

Fig. 5. REEs extraction at different residence times for the mixture Dy Nd La at pH = 1 by Cy 572 extractant in microfluidic device at 20 ± 2 °C. Dots and lines represent experimental and simulated data, respectively.

Fig. 5 shows the performance of the extraction process of an aqueous solution containing a mixture of dysprosium, neodymium and lanthanum, each with an initial concentration of 1 mM, as a function of the residence time in the microdevice. The experiment was carried out under controlled conditions of pH 1, strategically chosen to promote the selective separation of the rare earth elements.

The results obtained experimentally validate the CFD model and demonstrate its applicability in the design of microdevices capable of achieving a highly efficient extraction of dysprosium, reaching approximately 95 % at significantly low residence times. This performance highlights the high affinity of the system for this ion, as well as the effectiveness of the microdevice design under these conditions. On the other hand, neodymium extraction was much lower, with values below 10 %, while lanthanum extraction was practically null, allowing its effective separation.

These results highlight the predictive capability of the CFD model, which reproduces with high fidelity the performance of the microdevice under different operating scenarios. This confirms CFD simulation as an important tool not only for understanding the transport phenomena involved, but also for assisting in the design and sizing of microdevices that satisfy specific separation and performance requirements.

4.3. Evaluation of the microfluidic platform for the separation of mixtures of REEs

For the separation of a mixture of rare earth elements, specifically a ternary mixture composed of dysprosium, neodymium and lanthanum with a concentration of 1 mM of each element, it is essential to implement selective extraction and back-extraction stages. The number of these stages plays a crucial role in the final performance of REEs separation.

This study analyses a microfluidic process to provide a target yield of separation and recovery for each REE. In this case, the objective is to end with three streams enriched in a specific element (Dy, Nd, and La), to achieve a minimum recovery of 90 % of the REEs present in the feed and to ensure that each stream achieves a purity in the target REE higher than 90 %, as shown in the objectives displayed in Table 1:

4.3.1. Scenario 1

In the case of a ternary mixture, the minimum number of reactive stages required to achieve the separation of Dy, Nd, and La is 4, 2 for the extraction and 2 for the back-extraction process. Therefore, as a first approximation, the microfluidic platform was designed with 4 microextractors, one for each stage.

Fig. 6 shows the optimal configuration for the extraction and separation of this mixture. The first extraction, denoted as "E1", is performed at pH 1, where most dysprosium is extracted, remaining the other two elements in the aqueous phase. Subsequently, the pH of this phase is adjusted by addition of an aqueous stream with pH = 14 (aqueous stream 6). The remaining elements are conducted to a second extraction stage, "E2", which is carried out at pH 2.4, where most neodymium is

Table 1
Feed conditions and specific objectives of the separation process.

	Concentration (mM)			Purity (%)			Recovery (%)		
	Dy	Nd	La	Dy	Nd	La	Dy	Nd	La
Feed	1	1	1	33.3	33.3	33.3	–	–	–
Objective	> 1	> 1	> 1	90.0	90.0	90.0	90.0	90.0	90.0

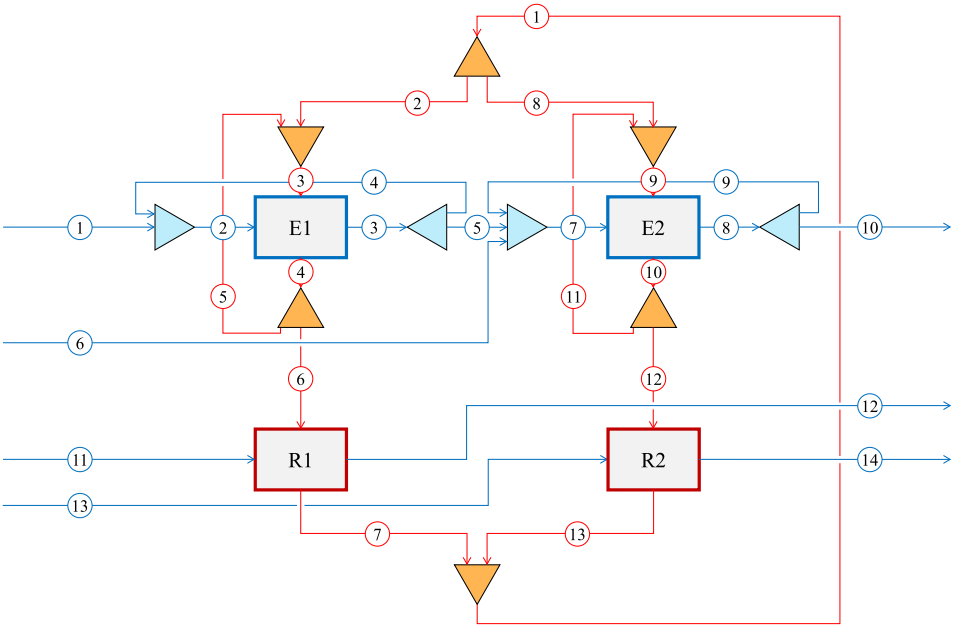

Fig. 6. Optimal microfluidic platform solution for the extraction-separation process of the Dy-Nd-La mixture, with recirculation streams in the extraction stages, both for the AP (aqueous streams 4 and 9) and for the OP (organic streams 5 and 11). This allows loading the OP and increasing the concentration of REEs before back-extraction.

extracted and the extraction of lanthanum is minimised.

The back-extraction stages are performed under acidic conditions to recover and concentrate the REEs in separated aqueous streams. The first back-extraction, "R1", recovers and concentrates dysprosium using a high proton concentration solution (3 M). The second back-extraction stage, "R2", recovers and concentrates neodymium working with 0.5 M proton concentration. These two stages recover practically all the REEs, eliminating the need for recirculation of the streams and allowing the organic phase to be reused without affecting the performance of the process. Moreover, these back-extraction stages are performed working with 30 % holdup of the aqueous phase (H_{AP}), concentrating the REEs and minimising the flow rate of the acidic streams.

Finally, lanthanum is recovered in the aqueous stream number 10 without the need to be further extracted and back-extracted, simplifying the process.

With the proposed configuration, a high separation yield of the three elements is achieved, reaching purities higher than 80 %, as illustrated in Fig. 7. The highest purity is obtained for dysprosium, with 98.1 %, due to its favourable isotherm compared to the other elements. This high purity of dysprosium reflects the effectiveness of the extraction and back-extraction conditions used in the process.

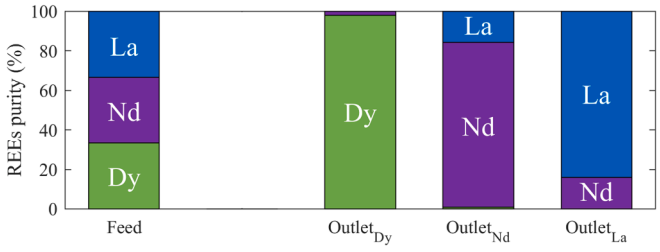

Fig. 7. Comparison between the feed and the outlet purity of each rare earth element (REE) in the microfluidic platform.

In contrast, the purities of neodymium and lanthanum are slightly lower, 83.3 % and 84.4 %, respectively. These results are due to the greater difficulty in separating these two elements, which leads to some cross-contamination. Part of the neodymium is transported to the lanthanum-rich stream and vice versa, which limits the final purity of both products.

This phenomenon is explained by the characteristics of the equilibrium curves (Fig. 4) and the selectivity of the reagents used in the extraction and back-extraction stages. The separation between neodymium and lanthanum is less effective due to the proximity of their physicochemical properties, which requires greater control and optimisation of the operating conditions.

Fig. 8 presents the concentrations of the rare earth elements at the inlet of the process (1 mM with a flow rate of 1.44 mol·day^{-1}) and at every outlet stream. It is observed that dysprosium is concentrated up to 12.4 mM with a flow rate of 1.41 mol·day^{-1}, while neodymium reaches a concentration of 42.7 mM with a flow rate of 1.18 mol·day^{-1}. The increase in dysprosium and neodymium concentrations is achieved by working with an H_{AP} of 70 % in the extraction stages and 30 % in the back-extraction stages, complemented by recirculation of both phases during extraction.

Lanthanum, on the other hand, leaves the process with a reduced concentration of 0.77 mM, due to the dilution in the pH adjustment step, reaching an outflow of 1.22 mol·day^{-1}. To increase the lanthanum concentration, it is recommended to incorporate two additional micro-devices, one for extraction and the other for back-extraction of this REE,

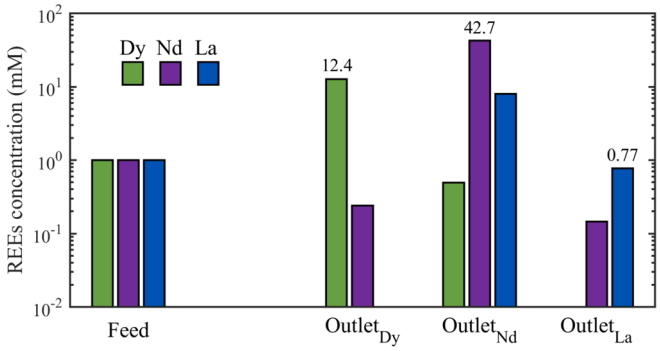

Fig. 8. Comparison between the feed and the outlet concentration of Dy, Nd, and La in the microfluidic platform.

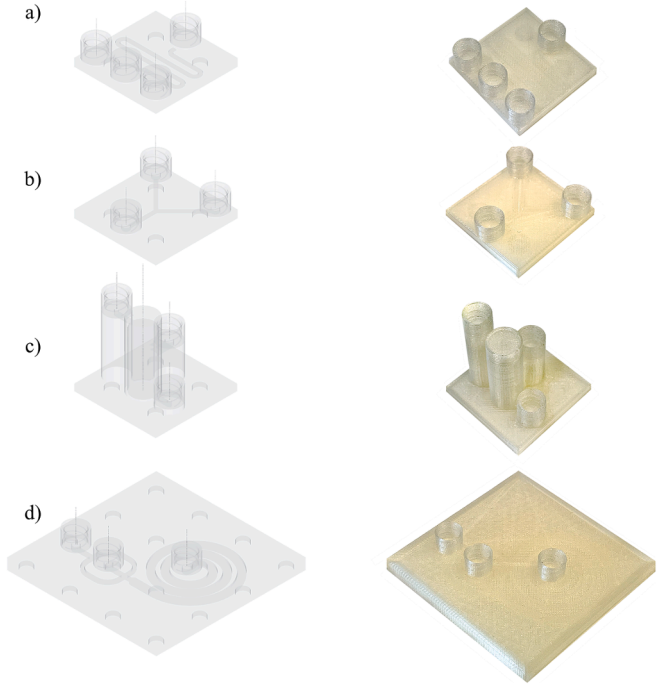

Fig. 9. Comparison between LEGO®-type microfluidic device designs (left) and fabrication (right) using 3D printing techniques: (a) mixer, (b) splitter, (c) settler, and (d) flow-focusing microextractor.

thus optimising its recovery in the process.

Lastly, when analysing the recovery rate for each REEs, it is observed that the retrieval of dysprosium is almost total, reaching 98.2 %. However, the recoveries of neodymium and lanthanum are lower, with values of 82.0 % and 84.4 %, respectively. This is due to the difficulty in achieving high separation yield between these two elements in a single stage, as shown in the equilibrium curves in Fig. 4. These curves evidence the complexity associated to the selectivity of the process, which underlines the need to add more stages to the process to improve the recovery of neodymium and lanthanum.

4.3.1.1. Manufacture of a modular microfluidic platform by 3D printing. The microfluidic platform was 3D printed from designs created in Autodesk Inventor® for every device. The microdevices, in which the extraction and back-extraction processes of the REEs take place have a flow-focusing configuration for the generation of aqueous droplets (Fig. 9.d), that flow along a microchannel with an Archimedean spiral geometry to the outlet of the microreactor. The settling blocks collect the two outflowing phases from the microreactors and allow them to be separated by settling in a cylindrical vessel (Fig. 9.c). The AP, due to its higher density, is settled at the bottom, while the OP, due to its lower density, accumulates at the top. The mixers are designed to homogenise the incoming streams of each phase by means of a microchannel in a serpentine shape before the streams leave the device (Fig. 9.a). Finally, the splitters divide the inlet phase into two or more streams with a specific flow rate at every outlet (Fig. 9.b).

This integrated design ensures efficient microfluidic processes with precise control of phase splitting, mixing and separation. It also allows the modular construction of an optimal REEs separation process on a small size platform. Fig. 10 illustrates the optimal flowsheet with four microextractors and the top view of the microfluidic platform designed to replicate this configuration. This modular approach not only makes the process easier to implement and fine-tune, but also improves its adaptability for future optimisation or scale-up.

The configuration used in this study consists of four microextractors (two for extraction and two for back-extraction), accompanied by four settling blocks for phase separation at the outlet of each microextractor. In addition, five mixers (two for the AP and three for the OP) and five flow splitters (two for the aqueous phase and three for the organic one) are integrated to facilitate streams recirculation within the process. All microdevices are connected using Luer Lock connectors and Tygon® tubing, with blue indicating the AP, red the OP and green the biphasic streams. These devices are fixed to a base by specially designed studs, ensuring effective distribution and quick and easy installation of the system components.

Fig. 11 illustrates how the optimised design of the microfluidic platform can be transferred to the experimental environment with high precision using 3D printing techniques. This allows for a modular platform with compact dimensions, which facilitates the construction and modification of processes using multiple microdevices in a fast and effective manner. In this case, the separation process of Dy, Nd and La has been implemented and optimised to operate with the minimum number of microreactors.

4.3.1.2. Validation of the optimization model. To assess the robustness of the mathematical model developed to optimise the microfluidic platform, Scenario 1 has been validated experimentally through batch trials. In these experiments, the concentrations of the compounds are measured at the inlet and outlet of each of the reactive stages of the process. The experimental results obtained are presented in Table 2 together with the estimates generated by the model.

A comparison of the two sets of data shows that the mathematical model predicts the performance of the process with an error less than 15 %, which is considered acceptable. A significant part of this error can be attributed to experimental factors such as variations in the concentration of REEs in the feed stream, variations in operating conditions during the tests and the accuracy limitations of the analytical techniques. Despite these sources of error, the model is able to capture the key aspects of the process and provides a reliable approach for prediction and optimisation of the microfluidic platform.

Consequently, this model is presented as a useful tool to reduce the reliance on physical experiments in future stages of development, allowing initial predictions to be made, saving both time and resources.

4.3.2. Scenario 2

In this study, different microfluidic platform configurations (scenarios) are analysed by varying both the number of microdevices and the configuration of streams within the process to achieve the criteria set out in Table 1. Each scenario explores specific combinations of microdevices and stream settings to optimise the process separation performance. This systematic evaluation allows the identification of the most appropriate configuration to meet the stablished objectives.

This scenario proposes the addition of four more microreactors to the four used in the previous one, making a total of eight (four for extraction and four for back-extraction), with the aim of improving the results. In

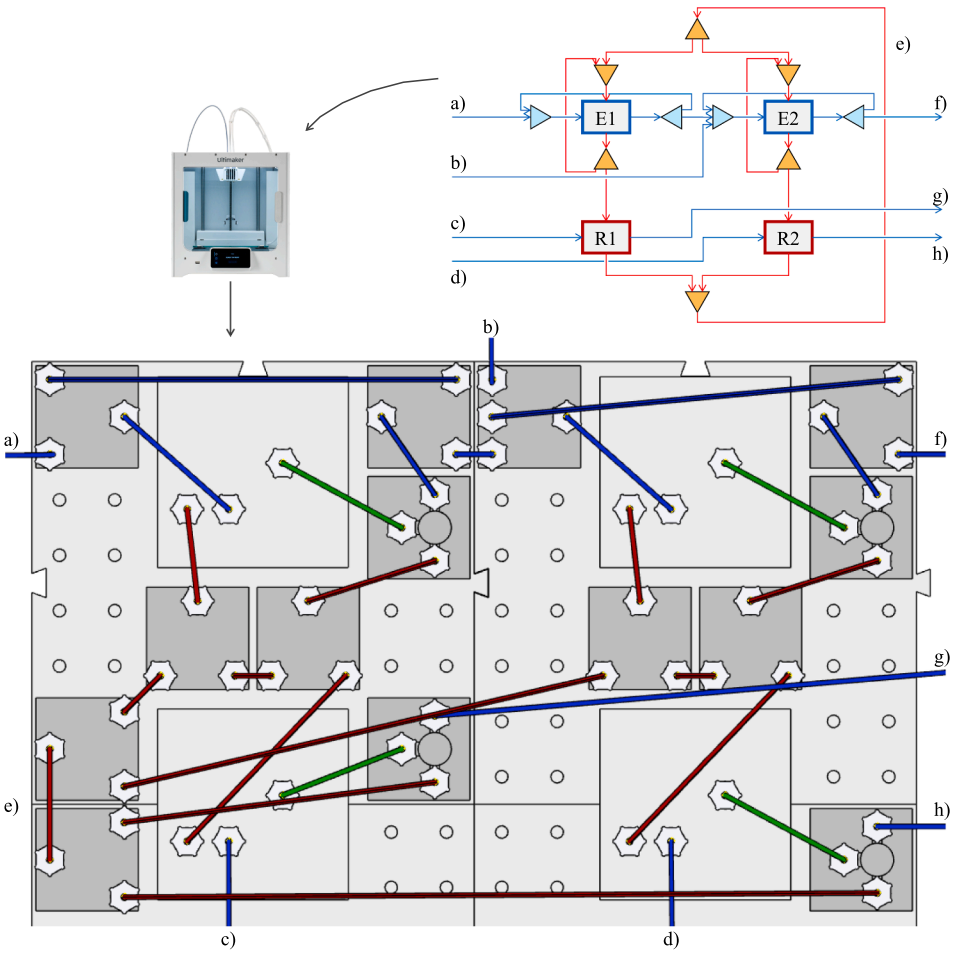

Fig. 10. Microfluidic platform fabricated, featuring distinct streams: aqueous feed (a), pH adjustment stream (b), aqueous acidic streams (c) and (d), recycled organic stream (e), outlet streams concentrated in La^{3+}(f), Dy^{3+}(g), and Nd^{3+}(h).

particular, the aim is to increase the recovery of all REEs and to concentrate lanthanum in the outlet stream without compromising the separation yield of the other elements.

The optimal configuration is shown in Fig. 12. First, dysprosium is separated in the extraction block E1 at pH 1, followed by its recovery in block R1 (9.2 M of HCl). Next, neodymium is separated in two extraction steps, E2 and E3, at pH 1.28 and 1.45, respectively, and then recovered in blocks R2 (pH = 0.81) and R3 (pH = 0.83). Finally, lanthanum is extracted in E4 at pH 4.49 and recovered in R4 (pH = 1.38), whichallows its concentration to be increased, leaving the aqueous stream (14) free of REE.

The extractors operate with an AP holdup of 70 % and 30 % for the back-extractors to improve the concentration of the elements. This concentration is further optimised by the recirculation of the OP in the extraction stages, which allows the recovery of the largest amount of REEs before back-extraction. Recirculation of the AP is also carried out in all extraction stages except in the first one (E1), as dysprosium is easier to be separated.

This configuration achieves purities above 90 % for all rare earth elements (Fig. 13), which represents a significant improvement in the separation process.

Dysprosium is obtained with a purity of 97.5 %, indicating a high separation performance of this element. Furthermore, the most remarkable improvements compared to the configuration previously studied are observed in the purities of neodymium and lanthanum, which reach values of 93.8 % and 96.4 %, respectively. These results show that the optimisation of the process, thanks to the correct configuration of the eight extraction and back-extraction stages, together with the recirculation of the organic and aqueous phases, has allowed both achieving a high-performance separation and high purity of the recovered REEs streams.

On the other hand, the rare earth elements leave the process with a concentration at least six times higher than the feed concentration, demonstrating the effectiveness of the proposed configuration (Fig. 14). Dysprosium is the element that reaches the highest concentration with 12.6 mM and a molar flow rate of 1.42 mol·day^{-1}, standing out as the component with the highest recovery. Neodymium, although with a lower final concentration of 6.14 mM, achieves a molar flow rate of 1.33 mol·day^{-1}, maintaining an adequate balance between concentration and recovery.

The additional extraction stage of lanthanum (E4), followed by its back-extraction in R4, has a key influence on the overall performance of the process, generating a molar flow rate of 1.34 mol·day^{-1} and reaching a concentration of 7.72 mM. This increase in lanthanum concentration, achieved without compromising the purity of the other elements, is particularly relevant as in the previous scenario the lanthanum separation and concentration was lower, to the detriment of the other REEs recovery.

The current configuration not only maximises the recovery of lanthanum but also solves the previously observed concentration/purity trade-off. The balance between the outlet molar flow rates and the high concentration of REEs ensures a high-performance process in terms of both separation and recovery. These results confirm that the recirculation of the organic and aqueous phases, together with additional stages for the recovery of specific elements such as lanthanum, contribute significantly to the improvement of the process without negatively

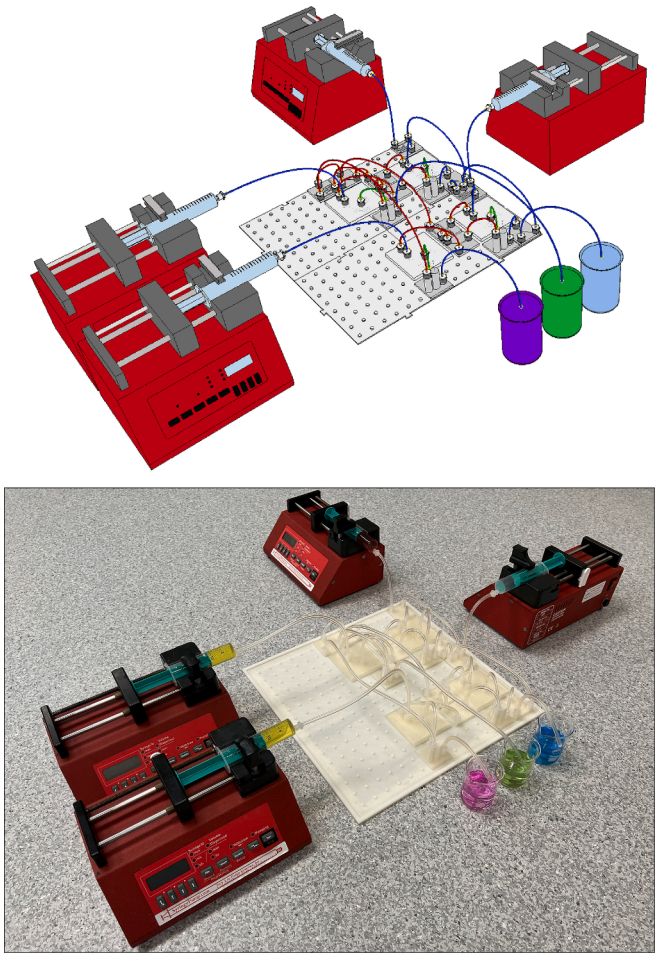

Fig. 11. Comparison between Autodesk Inventor® 3D microfluidic platform design and the final manufactured system.

affecting the quality of the final product.

Overall, Scenario 2 offers the best configuration in terms of REEs concentration and purity, ensuring high REE recovery of more than 90 %. In this optimised configuration, the remarkable recovery of dysprosium (98.5 %) underlines the high performance of the process in the separation of this element, which is critical in several technological applications, such as the manufacture of high-performance permanent magnets. Neodymium recovery, although slightly lower, remains at a high recovery level of 92.6 %, indicating that the design of the process has improved its recovery without compromising its purity. Lanthanum recovery, at 93.3 %, also reflects a significant improvement, especially compared to the previous scenario where the focus on its concentration resulted in lower overall recoveries.

As listed in Table 3, the results obtained in the different scenarios indicate that it is possible to carry out the separation of the three rare earth elements using four microextractors, thus achieving the objectives set for dysprosium. However, this configuration has limitations that impede the achievement of the objectives proposed for neodymium and lanthanum. In response to this situation, a second scenario is proposed in which the number of microextractors is increased to eight. This design proved to be very effective in the separation of REEs and met all the established objectives, constituting the optimal solution. However, it should be noted that this is the most complex configuration and requires more equipment.

These results show that the developed tool not only optimises the separation process but also allows precise setting according to the defined objectives. The tool's ability to analyse and simulate different scenarios facilitates the identification of optimal conditions that maximise elements' recovery and purity. Furthermore, its implementation can contribute significantly to the overall performance of the process, minimising the time and resources required.

5. Conclusions

This research stems from the need to develop a system composed of microdevices capable of performing the optimal separation of different elements of interest. As a result, an easily adaptable and scalable microfluidic platform has been designed, which has allowed significant advances in the recovery and purity of the elements studied (Dy, Nd, La). The developed mathematical model has been experimentally validated and proved to be able to optimise the separation using a minimum number of four microextractors, achieving a purity higher than 83 % and recoveries of 82 % for each REE. Additional microextractors improve the separation between Nd and La, increasing the purity of these elements

Table 2
Comparison of the results obtained from the optimisation model (Sim) and the experimental results (Exp).

	Aqueous phase					Organic phase				
	ID	Dy^{3+}	Nd^{3+}	La^{3+}	pH	ID	$DyA_3(HA)_3$	$NdA_3(HA)_3$	$LaA_3(HA)_3$	$(HA)_2$
	(-)	(mM)	(mM)	(mM)	(-)	(-)	(mM)	(mM)	(mM)	(mM)
Sim	①	1.00	1.00	1.00	1.00	③	3.62	0.144	$2.60\cdot10^{-3}$	289
Exp		1.04	0.901	0.854	1.00		3.72	0	0	289
Sim	⑤	0.161	1.02	1.00	0.989	④	5.43	0.103	$3.43\cdot10^{-3}$	283
Exp		0.242	0.854	0.846	0.989		5.44	0.101	$1.77\cdot10^{-2}$	283
Sim	⑥	0	0	0	14.0	⑦	$2.10\cdot10^{-2}$	$1.20\cdot10^{-6}$	$1.35\cdot10^{-9}$	300
Exp		0	0	0	14.0		0.189	$3.60\cdot10^{-2}$	$1.19\cdot10^{-2}$	299
Sim	⑩	$9.88\cdot10^{-5}$	0.145	0.769	2.14	⑨	4.06	17.6	3.15	225
Exp		$8.63\cdot10^{-3}$	$8.09\cdot10^{-2}$	0.689	2.21		4.18	16.8	2.99	229
Sim	⑪	0	0	0	-0.477	⑩	4.38	19.3	3.45	219
Exp		0	0	0	-0.474		4.68	18.4	3.33	218
Sim	⑫	12.6	0.241	$7.77\cdot10^{-3}$	-0.471	⑬	4.17	1.09	$6.92\cdot10^{-3}$	284
Exp		12.2	0.152	$1.41\cdot10^{-2}$	-0.468		4.50	2.27	0.277	276
Sim	⑬	0	0	0	0.523					
Exp		0	0	0	0.523					
Sim	⑭	0.491	42.6	8.05	0.788					
Exp		0.422	37.7	7.13	0.785					

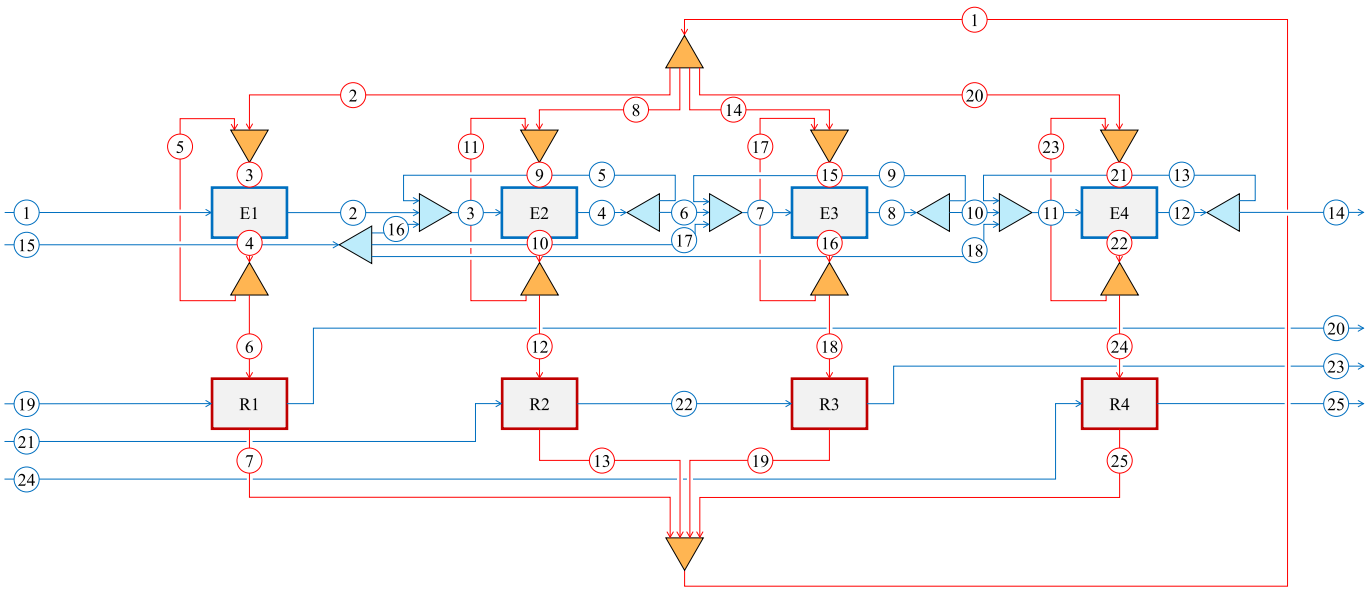

Fig. 12. Optimal flowsheet of the microfluidic platform for the extraction-separation process of the Dy-Nd-La mixture in Scenario 2, composed by 4 extraction and 4 back-extraction stages.

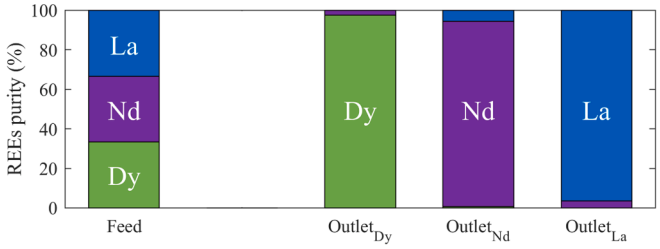

Fig. 13. Purity achieved in Scenario 2: Comparison between feed and outlet purity for each rare earth element (REE) in the microfluidic platform.

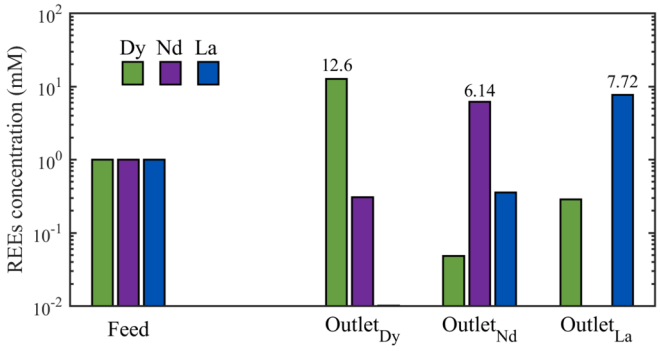

Fig. 14. Concentration of REEs achieved in Scenario 2: Comparison between feed and outlet concentration of Dy, Nd, and La in the microfluidic platform.

over 93 %.

Working with eight microextractors increases the complexity of the separation process but significantly improves the purity and recovery of all three elements with recoveries over 92 %. This demonstrates the flexibility and scalability of the system to adapt to different performance levels.

The modular design and optimisation of the process not only improves the quality of the final product but also reduces the use of reagents by recirculating the liquid phases, improving resource efficiency in the process. Although increasing the number of stages in the process improves the recovery yield and helps to achieve the separation objective, this approach also leads to increased costs associated to equipment and infrastructure required in the process scale up. Therefore, the optimum design must be adapted to the separation objectives.

The microextraction platform, designed with a 3D printed LEGO®-type microdevices, offers a high degree of modularity, allowing the system to be quickly reconfigured for different separation objectives. This makes it easy to adapt to different applications, making it a low-cost tool for assessing the modularity of the separation process. However, it should be borne in mind that each new application requires a previous specific design stage of the microdevices, assisted by CFD simulations, in order to ensure optimal system performance.

In summary, the constructed microfluidic platform and developed optimisation model represent a significant advance in the high-performance separation of critical materials, combining high purity and recovery with design flexibility. These results consolidate the use of microfluidic technology as a promising tool for processes involving the separation of fluid phase mixtures.

Table 3
Feed conditions and process results working with different configurations.

	Concentration (mM)			Purity (%)			Recovery (%)		
	Dy	Nd	La	Dy	Nd	La	Dy	Nd	La
Feed	1	1	1	33.3	33.3	33.3	–	–	–
Objective	> 1	> 1	> 1	90.0	90.0	90.0	90.0	90.0	90.0
Scenario 1	**12.4**	**42.7**	0.77	**98.1**	83.3	84.4	**98.2**	82.0	84.4
Scenario 2	**12.6**	**6.14**	**7.72**	**97.5**	**93.8**	**96.4**	**98.5**	**92.6**	**93.3**

CRediT authorship contribution statement

Christian Fernández-Maza: Conceptualization, Formal analysis, Investigation, Methodology, Software, Validation, Visualization, Writing – original draft. **Gloria González-Lavín:** Formal analysis, Investigation, Methodology, Software, Writing – review & editing. **Lucía Gómez-Coma:** Conceptualization, Methodology, Supervision, Writing – review & editing. **Marcos Fallanza:** Conceptualization, Formal analysis, Methodology, Software, Supervision, Writing – review & editing. **Inmaculada Ortiz:** Conceptualization, Formal analysis, Funding acquisition, Project administration, Resources, Supervision, Writing – review & editing.

Declaration of competing interest

The authors declare that they have no known competing financial interests or personal relationships that could have appeared to influence the work reported in this paper.

Acknowledgments

This work received financial assistance from project PID2021-123120OB-I00 funded by MICIU/AEI/ 10.13039/501100011033 and ERDF/EU, and project PDC2022-133122-I00 funded by MICIU/AEI/ 10.13039/501100011033 and the European Union NextGenerationEU/ PRTR. Gloria González-Lavín gratefully acknowledges grant FPU21/ 03297 funded by MICIU/AEI/10.13039/501100011033 and ESF+.

Data availability

Data will be made available on request.

References

[1] C. Fernández-Maza, G. González-Lavín, L. Gómez-Coma, M. Fallanza, I. Ortiz, High performance flow-focusing droplet microreactor. Extractive separation of rare earths as case of study, Chem. Eng. J. 486 (2024), https://doi.org/10.1016/j.cej.2024.150136.
[2] C. Fernández-Maza, M. Fallanza, L. Gómez-Coma, I. Ortiz, Performance of continuous-flow micro-reactors with curved geometries. Experimental and numerical analysis, Chem. Eng. J. 437 (2022), https://doi.org/10.1016/j.cej.2022.135192.
[3] G. González-Lavín, B. García-Merino, C. Fernández-Maza, E. Bringas, L. Gómez-Coma, M. Fallanza, I. Ortiz, Tailored Euler-Lagrange modelling of microfluidic solid/liquid reactive separations, Chem. Eng. J. 495 (2024), https://doi.org/10.1016/j.cej.2024.153393.
[4] A. Farahani, A. Rahbar-Kelishami, H. Shayesteh, Microfluidic solvent extraction of Cd(II) in parallel flow pattern: Optimization, ion exchange, and mass transfer study, Sep. Purif. Technol. 258 (2021) 118031, https://doi.org/10.1016/j.seppur.2020.118031.
[5] Y. Zhou, Z. Chen, A. Chen, J. Zhang, X. Wu, J. Xu, Comprehensive recovery of NCM cathode materials for spent lithium-ion batteries by microfluidic device, Sep. Purif. Technol. 294 (2022) 121185, https://doi.org/10.1016/j.seppur.2022.121185.
[6] P. Abdollahi, J. Karimi-Sabet, M.A. Moosavian, Y. Amini, Microfluidic solvent extraction of calcium: Modeling and optimization of the process variables, Sep. Purif. Technol. 231 (2020) 115875, https://doi.org/10.1016/j.seppur.2019.115875.
[7] M. Wouters, S. Rahman, H. Myamoto, N.N. Tran, V. Hessel, Continuous microfluidic solvent extraction of cobalt from mimicked and real asteroid leaching solutions, Sep. Purif. Technol. 260 (2021) 118238, https://doi.org/10.1016/j.seppur.2020.118238.
[8] J. Wen, H. Liu, J. Luo, J.M. Schulz, L. Böhm, X. Wang, P. Ning, Mass transfer characteristics of vanadium species on the high-efficient solvent extraction of vanadium in microchannels/microreactors, Sep. Purif. Technol. 315 (2023) 123638, https://doi.org/10.1016/j.seppur.2023.123638.
[9] K. Cui, K. Huang, Controlling flow patterns and its evolution behavior in microchannel for intensified separation of rare-earth and Al(III) ions: Hints from the hydrodynamics parameters, Sep. Purif. Technol. 277 (2021) 119401, https://doi.org/10.1016/j.seppur.2021.119401.
[10] Z. Chen, W.T. Wang, F.N. Sang, J.H. Xu, G.S. Luo, Y.D. Wang, Fast extraction and enrichment of rare earth elements from waste water via microfluidic-based hollow droplet, Sep. Purif. Technol. 174 (2017) 352–361, https://doi.org/10.1016/j.seppur.2016.10.059.
[11] L. Omodara, S. Pitkäaho, E.M. Turpeinen, P. Saavalainen, K. Oravisjärvi, R. L. Keiski, Recycling and substitution of light rare earth elements, cerium, lanthanum, neodymium, and praseodymium from end-of-life applications - A review, J. Clean. Prod. 236 (2019) 117573, https://doi.org/10.1016/j.jclepro.2019.07.048.
[12] P. Ram, R. Singhal, G. Choudhary, R.K. Sharma, On the key role of Dy3 + in spinel LiMn2O4 cathodes for Li-ion rechargeable batteries, J. Electroanal. Chem. 802 (2017) 94–99, https://doi.org/10.1016/j.jelechem.2017.08.052.
[13] Ó. Barros, P. Parpot, E. Rombi, T. Tavares, I.C. Neves, Machine learning approach for classification of REE/Fe-zeolite catalysts for fenton-like reaction, Chem. Eng. Sci. 285 (2024) 119571, https://doi.org/10.1016/j.ces.2023.119571.
[14] J. Priya, N.K. Gondia, A.K. Kunti, S.K. Sharma, Pure white light emitting tetrakis β-diketonate dysprosium complexes for OLED applications, ECS J. Solid State Sci. Technol. 5 (2016) R166–R171, https://doi.org/10.1149/2.0101610jss.
[15] D. Gielen, Critical materials for the energy transition, Abu Dhabi, 2021.
[16] J. Yano, T. Muroi, S. Ichi Sakai, Rare earth element recovery potentials from end-of-life hybrid electric vehicle components in 2010–2030, J. Mater. Cycles Waste Manag. 18 (2016) 655–664, https://doi.org/10.1007/s10163-015-0360-4.
[17] V. Balaram, Rare earth elements: A review of applications, occurrence, exploration, analysis, recycling, and environmental impact, Geosci. Front. 10 (2019) 1285–1303, https://doi.org/10.1016/j.gsf.2018.12.005.
[18] F. Xie, T.A. Zhang, D. Dreisinger, F. Doyle, A critical review on solvent extraction of rare earths from aqueous solutions, Miner. Eng. 56 (2014) 10–28, https://doi.org/10.1016/j.mineng.2013.10.021.
[19] E. Pariset, C. Pudda, F. Boizot, N. Verplanck, F. Revol-Cavalier, J. Berthier, A. Thuaire, V. Agache, Purification of complex samples: Implementation of a modular and reconfigurable droplet-based microfluidic platform with cascaded deterministic lateral displacement separation modules, PLoS One 13 (2018) 1–18, https://doi.org/10.1371/journal.pone.0197629.
[20] L.J. Millet, J.D. Lucheon, R.F. Standaert, S.T. Retterer, M.J. Doktycz, Modular microfluidics for point-of-care protein purifications, Lab Chip. 15 (2015) 1799–1811, https://doi.org/10.1039/c5lc00094g.
[21] E.J. Fong, C. Huang, J. Hamilton, W.J. Benett, M. Bora, A. Burklund, T.R. Metz, M. Shusteff, A microfluidic platform for precision small-volume sample processing and its use to size separate biological particles with an acoustic microdevice, J. vis. Exp. 105 (2015) 1–11, https://doi.org/10.3791/53051.
[22] N. Sen, R. Chakravarty, K.K. Singh, S. Chakraborty, K.T. Shenoy, Selective separation of Cu from large excess of Zn using a microfluidic platform, Chem. Eng. Process. - Process Intensif. 159 (2021) 108215, https://doi.org/10.1016/j.cep.2020.108215.
[23] CYTEC, CYANEX® 572 Product Data Sheet, (2013).
[24] S. Rahmati, R. Adavodi, P. Romano, F. Vegliò, Evaluation of the mechanisms of rare earth elements extraction from citrate solutions in the recycling of NdFeB magnets, Process Saf. Environ. Prot. 195 (2025) 106788, https://doi.org/10.1016/j.psep.2025.106788.
[25] N.E. El-Hefny, M.S. Gasser, S.S. Emam, W.H. Mahmoud, H.F. Aly, Comparative studies on Y(III) and Dy(III) extraction from hydrochloric and nitric acids by Cyanex 572 as a novel extractant, J. Rare Earths. 36 (2018) 1342–1350, https://doi.org/10.1016/j.jre.2018.04.012.